Applied Catalysis B: Environmental 150–151 (2014) 204–217

Contents lists available at ScienceDirect

Applied Catalysis B: Environmental

journal homepage: www.elsevier.com/locate/apcatb

Investigation of the nature of silver species on different Ag-containing NO_x reduction catalysts: On the effect of the support

Rui Bartolomeu[a,b], Bruno Azambre[c], Alexandre Westermann[c], Auguste Fernandes[a], Raquel Bértolo[a], Houeida Issa Hamoud[c], Carlos Henriques[a], Patrick Da Costa[b], Filipa Ribeiro[a,*]

[a] Instituto Superior Técnico, Institute for Biotechnology and Bioengineering, Centre for Biological and Chemical Engineering, Av. Rovisco Pais, 1049-001 Lisboa, Portugal
[b] Université Pierre et Marie Curie, Paris 6, Institut Jean Le Rond d'Alembert, CNRS UMR 7190, 2 Place de la Gare de Ceinture, 78210 Saint Cyr l'école, Paris, France
[c] Laboratoire de Chimie et Physique—Approche Multi-échelle des Milieux Complexes, EA 4632, Institut Jean Barriol, Université de Lorraine, Rue Victor Demange, 57500 Saint-Avold, France

ARTICLE INFO

Article history:
Received 6 October 2013
Received in revised form
27 November 2013
Accepted 13 December 2013
Available online 25 December 2013

Keywords:
Silver
Alumina
Ceria–zirconia
ZSM-5 zeolite
SCR

ABSTRACT

Silver species present in four different Ag-based catalysts, with different supports (Al_2O_3, ceria–zirconia, sulphated ceria–zirconia and MFI zeolite), were identified by a combination of different characterization techniques (Powder XRD, Raman Spectroscopy, TEM, H_2-TPR, DRS UV–Vis Spectroscopy, CO adsorption followed by DRIFTS and pyridine adsorption followed by FTIR), each one allowing to obtain information on specific Ag species. While Powder XRD and Raman gave structural information on the Ag species present on the catalysts, complementary information on their relative reducibility and electronic state was obtained by H_2-TPR, DRS UV–Vis and CO adsorption followed by DRIFTS.

The possibility of different redox cycles occurring during the NO_x SCR reaction between the silver species present in each catalyst was discussed.

1. Introduction

Among Ag-based catalysts, Ag/Al_2O_3 has been studied by several authors in the NO_x SCR reaction with ethanol [1,2], being able to attain high NO_x conversions. Optimal Ag content of this high performance catalyst seems to be around 2.5 wt% [2,3]. Several authors have thoroughly studied this catalyst, paying special attention on one hand to its reactivity (intermediate chemistry and reaction mechanism) [4–6] and on the other hand to the Ag species stabilized on the Al_2O_3 support [7,8].

In a previous study [9], ceria–zirconia (CZ) and sulphated ceria–zirconia (SCZ) catalysts have shown mild NO_x SCR with ethanol activity, with SCZ showing an improvement relatively to the non-sulphated CZ. However, when Ag was introduced on SCZ, low temperature NO_x conversion decreased, while high temperature NO_x conversion slightly increased [10] in comparison with the sulphated support alone. This led to the conclusion that the Ag species present on the Ag/SCZ catalyst (namely Ag_2SO_4 and other non-identified oxidized Ag species) were not essential for the NO_x SCR reaction, having a positive or negative effect on the catalyst activity depending on the Ag-containing phase present under reaction conditions. From the TPSR profiles obtained on the above-mentioned study, Ag introduction seemed to promote instead ethanol conversion into acetaldehyde and CO_2, while decreasing CO formation.

On the other hand, Ag/zeolite catalysts have been reported to achieve interesting NO_x conversions using propane or ethanol as reducing agent [11,12]. These catalysts attain higher NO_x conversions than the non-exchanged zeolite support, but lower than those obtained for the Ag/Al_2O_3 catalyst. The MFI zeolite was chosen as support since it has been reported as one of the most active zeolite structures, when ion-exchanged with about 4 wt% Ag [13]. In addition, zeolites present unique ion-exchange properties that the other supports do not have.

According to the literature, Ag introduction on these supports can lead to the formation of a wide array of Ag species. The reactivity of these Ag species in NO_x SCR is still matter of debate in the literature, with authors proposing different Ag species to be active

* Corresponding author. Tel.: +351 21 841 7872; fax: +351 21 841 9198.
E-mail address: filipa.ribeiro@ist.utl.pt (F. Ribeiro).

0926-3373/$ – see front matter © 2013 Elsevier B.V. All rights reserved.
http://dx.doi.org/10.1016/j.apcatb.2013.12.021

Table 1
Ag species on Ag/Al_2O_3 and Ag/zeolite catalysts and their role during NO_x SCR.

Ag Species	Support	Technique	Reactivity	Reference
β-$AgAlO_2$	Al_2O_3	XRD, DRS UV–Vis, EXAFS	C_3H_6-SCR[a]	[7,14]
AgO	MFI, FAU	H_2-TPR	–	[15]
Ag_2O	Al_2O_3, MFI, FAU, MOR	H_2-TPR, XPS	C_3H_6-SCR, ethanol-SCR	[2,15–17]
Ag^+	Al_2O_3	H_2-TPR, DRS UV–Vis, EXAFS	decane-SCR, octane-SCR, C_3H_8-SCR	[3,18,19]
$Ag_n^{\delta+}$	Al_2O_3, MFI, BEA, FAU, MOR	H_2-TPR, DRS UV–Vis, EXAFS	decane-SCR, C_3H_8-SCR	[18,20]
Ag_m	MFI, BEA, FAU, MOR, ERI, LTL	DRS UV–Vis	HC combustion	[11,21]
Ag^0	Al_2O_3, MFI, BEA, FAU, MOR	XRD, TEM, DRS UV–Vis, XPS	HC combustion, NO_2 formation, N_2O formation	[7,11,17,22]

[a] Korhonen et al. [23] have recently discarded β-$AgAlO_2$ as the active species in C_3H_6-SCR.

for NO_x SCR. Table 1 summarizes the main Ag species reported in literature that can be found in Ag-based catalysts, in which support they were detected and their catalytic activity. It should be noted that, to the best of our knowledge, characterization of Ag species present on Ag/CZ catalysts has not yet been addressed in the literature.

Ag species can be divided into two main groups: oxidized (β-$AgAlO_2$, AgO, Ag_2O, Ag^+ and $Ag_n^{\delta+}$) and reduced Ag species (Ag_m and Ag^0). From Table 1, it can be concluded that the several Ag species proposed on literature, as active for NO_x SCR reaction, all belong to the first group. On the other hand, reduced Ag species are unequivocally associated to HC combustion, oxidation of NO to NO_2 and N_2O formation from NO.

Furthermore, the NO_x SCR reaction mechanism is quite complex and comprises several steps/cycles. In this regard, the following question arises: in which step(s) of the mechanism do the Ag species play a role? For example, since reduced Ag species catalyse NO_2 formation, which is the first step in NO_x SCR, these species can have an important role in the catalyst activity. For Ag/Al_2O_3 catalysts, Meunier et al. [22] have proposed a general mechanism which attributed different roles to the Ag species in the NO_x SCR with propene. Briefly, Ag^0 particles catalyse the NO decomposition-reduction, while Ag^+ species promote the formation of RNO_x species, intermediates of the N_2 formation reaction. Although the role of Al_2O_3 support on the formation/decomposition of these RNO_x species was not clear for these authors, subsequent studies from other authors have put into evidence a great mobility of some intermediate species between the Ag species and Al_2O_3 support [6,24]. Regarding Ag/zeolite catalysts, only Martens et al. [25] have postulated a reaction mechanism which attributed a concrete role to Ag species for NO_2 reduction with propene. It was assumed by these authors that the reduction of an RNO_x intermediate into an RNH_x species was part of an Ag^+/Ag^0 redox cycle, which was completed by HC partial and total oxidation. In addition, the Ag^+/Ag^0 pair is involved in different mechanism steps, disputing the existence of a single active oxidized Ag species and underlining the importance of reduced Ag species in the NO_x SCR reaction mechanism. A similar redox cycle was also postulated by Sazama et al. [18], but in this case between Ag^+ (or Ag_2O) and $Ag_n^{\delta+}$ species on an Ag/Al_2O_3 catalyst. However, these authors did not attribute a specific mechanism step to this Ag redox cycle.

Finally, Ag species identification presents some constraints, as it is the case of H_2-TPR and DRS UV–Vis, the characterization techniques more commonly described in the literature. While H_2-TPR is only able to identify oxidized Ag species, DRS UV–Vis does not detect Ag_2O [26]. Furthermore, peak assignment in H_2-TPR experiments is frequently contradictory in the literature, especially in the case of Ag_2O and Ag^+ differentiation [17]. As for DRS UV–Vis, band attributions greatly depend on the authors [27].

In this work we will focus on the characterization of Ag species in Ag/Al_2O_3 and comparison with the Ag species present on other Ag-based catalysts with different supports: CZ, SCZ and MFI zeolite. Since it is not possible to have a characterization technique that can encompass all possible Ag species, a combination of different techniques was used to allow a better analysis of the different Ag species present on the Ag-based catalysts. Hence, correlations will be attempted between the data collected from PXRD, Raman, TEM, H_2-TPR, DRS UV–Vis, and DRIFTS and FTIR measurements of adsorbed CO and pyridine, respectively, on the four Ag-based catalysts possessing different acidic and redox properties. Insights will be provided to better explain the behaviour of the Ag-containing catalysts in NO_x SCR with ethanol.

2. Experimental

2.1. Catalysts preparation

2.5Ag/Al_2O_3 catalyst was prepared by Excess Solvent Impregnation (ESI) of *Sasol 0.6/170* γ-Al_2O_3 spheres (S_{BET} = 170 m^2/g). ESI was carried out in a rotary evaporator device, with an $AgNO_3$ (*Sigma-Aldrich*) solution (volume of solution/catalyst weight (v/w) = 6 mL/g). The γ-Al_2O_3 spheres and the $AgNO_3$ solution were stirred in the rotary evaporator flask at 60 °C, under atmospheric pressure, for 30 min. Then, the excess solution was evaporated under vacuum at 60 °C, after which the catalyst was dried overnight in an oven at 100 °C and finally calcined at 500 °C for 2 h (heating rate of 10 °C/min). The Ag/Al_2O_3 spheres were then crushed in order to obtain a powder with a mean diameter around 5 μm. Ag content on this catalyst was 2.5 wt% Ag (ICP analysis).

The mixed ceria–zirconia oxide (CZ) support, with the formula $Ce_{0.21}Zr_{0.79}O_2$ (S_{BET} = 180 m^2/g) was supplied by *Solvay-Rhodia* (La Rochelle, France). The sulphated ceria–zirconia support (SCZ) was prepared according to the procedure described elsewhere [10] (S_{BET} = 184 m^2/g), resulting in a concentration of 1.7 wt% on SO_4^{2-} (elementary analysis).

3Ag/CZ and 3Ag/SCZ catalysts were prepared by Incipient Wetness Impregnation (IWI) of the CZ or SCZ supports, respectively, with an $AgNO_3$ (*Sigma-Aldrich*) solution with the adequate concentration in order to obtain solids containing 3 wt% Ag (verified by ICP analysis). Both catalysts were dried under vacuum at 70 °C and then calcined at 500 °C for 30 min (heating rate of 10 °C/min).

The parent NH_4MFI(25) zeolite, with Si/Al = 25, was supplied by *Zeolyst International*. This zeolite was converted to its protonic form

(HMFI(25)), by calcination at a heating rate of 5 °C/min, kept at 200 °C for 2 h and at 500 °C for 8 h (S_{BET} = 377 m^2/g).

4Ag/HMFI(25) catalyst was prepared by ion-exchanging three times parent NH_4MFI(25) zeolite with a 0.01 M $AgNO_3$ (*Sigma-Aldrich*) solution. Ion-exchange was carried out at room temperature (RT) for 24 h in the dark, to avoid Ag^+ reduction. The ratio between the volume of solution and the catalyst weight (v/w) was equal to 100 mL/g. After each ion-exchange the catalyst was washed with distilled water and dried at 100 °C overnight. Then, the catalyst was calcined following the same calcination procedure used to obtain HMFI(25) zeolite. Ag content on this catalyst was 4.1 wt% Ag (ICP analysis).

2.2. Catalysts characterization

The Ag-containing catalysts were characterized by PXRD (Powder X-ray Diffraction), Raman Spectroscopy, TEM (Transmission Electron Microscopy), H_2-TPR (Temperature Programmed Reduction), *in situ* DRS UV–Vis (Diffuse Reflectance UV–Vis Spectroscopy), CO adsorption followed by DRIFTS (Diffuse Reflectance Infrared Fourier Transformed Spectroscopy) and pyridine adsorption followed by FTIR (Fourier Transformed Infrared Spectroscopy).

PXRD patterns were collected on a *Bruker D8 Advance* diffractometer equipped with a graphite monochromator and using Cu-*Kα* radiation. A step size of 0.02° (2*θ*) and a step time of 12 s were employed during acquisition.

Raman spectra were collected between 200 and 3000 cm^{-1} on a *BWTek-i-Raman* portable spectrometer using a 785 nm laser without any sample pre-treatment. The laser power and time collection were optimized for each sample in order to optimize the signal while preserving the samples from burning locally.

TEM was performed on a *JEOLJEM 2011 HR (LaB6)* microscope operating at 200 kV. Prior to TEM, the sample was crushed and then dispersed without solvent addition on a carbon-coated copper TEM grid. According to Sayah et al. [28], solvent addition, such as ethanol, leads to reduction of the Ag species on the catalyst.

H_2-TPR experiments were performed on a *Micromeritics AutoChem II 2920*, using 80 mg of catalyst. Before each run, the sample was pre-treated under flowing air (flow rate of 25 mL/min) from RT to 500 °C (10 °C/min), kept at 500 °C for 1 h and then cooled to RT. Then, the reactor was purged with argon for 10 min at RT. H_2-TPR was carried out under a mixture of 5% H_2/Ar with a flow rate of 30 mL/min, from RT to 900 °C at a heating rate of 10 °C/min. Hydrogen consumption was measured with a TCD; water formed during reduction processes was trapped in a dry ice trap.

DRS UV–Vis spectra were collected on a *Varian Cary 5000 UV–Vis-NIR* spectrophotometer. A *Praying Mantis* accessory, coupled with a reaction chamber, allowed to perform measurements using a similar procedure to that used during H_2-TPR experiments, with an oxidation step, followed by a reduction treatment. *Spectralon*® was used as reference. During the oxidation step, the sample was heated from RT up to 500 °C (10 °C/min) under air flow, with spectra being collected with intervals of 100 °C between them. Then, the sample was cooled down to RT, still under air flow, and a final spectrum was collected. The reduction treatment was performed immediately after the oxidation step, on the same sample, after a He purge. The sample was heated from RT up to 500 °C (10 °C/min) under a flow of 5% H_2/He with spectra being collected with intervals of 100 °C between them. After that, the sample was cooled down to RT, still under a flow of 5% H_2/He, and a final spectrum was collected. A constant flow of 25 mL/min was used though all spectroscopic measurements.

RT CO adsorption followed by DRIFTS was performed on a *Varian Excalibur 4100* FTIR spectrophotometer equipped with a diffuse reflectance *Graseby Specac* optical accessory and a *Spectra-Tech* environmental chamber. Before each run, the sample was pre-treated under flowing He (flow rate of 60 mL/min) from RT to 450 °C (15 °C/min) and then cooled down to 30 °C. Background spectrum was recorded and 1000 ppm CO/He (30 mL/min) were introduced at 30 °C, in order to increasingly saturate the sample with CO while obtaining time-resolved spectra (co-addition of 100 scans with a resolution of 2 cm^{-1}).

Pyridine adsorption followed by FTIR was performed on a *Thermo Nicolet Nexus 470* spectrometer equipped with a DTGS detector. Each catalyst was pressed into thin wafers (5–10 mg/cm^2) and pre-treated in an *in-situ* IR cell, under secondary vacuum (10^{-6} torr) at 450 °C for 3 h. After the pre-treatment, a spectrum was recorded and then the sample was cooled down to 150 °C and saturated with pyridine vapour (2 torr) for 10 min. Excess pyridine was removed for 30 min under secondary vacuum (10^{-6} torr), after which a spectrum was recorded. Before each spectrum collection, a background spectrum was always recorded.

2.3. Catalytic tests

Temperature Programmed Surface Reaction (TPSR) and steady-state isothermal experiments were carried out in the same experimental setup and using the same procedure as described elsewhere [9]. A reaction mixture containing 1920 ppm NO + 3020 ppm ethanol + 5% O_2 (He) was fed to a 200 mg catalyst bed (GHSV = 50,000 h^{-1}). The composition of the reactor outflow was continuously monitored using a heated FTIR gas cell (*Cyclone Series—Specac*, optical path length = 2 m, *V* = 0.19 L) coupled to a *Varian Excalibur 4100* FTIR spectrometer with a DTGS detector. The temperature of the gas cell was maintained at 110 °C to avoid any condensation of the reactants/products during the tests. FTIR spectra, referenced to a He background, were recorded using a 2 cm^{-1} resolution and co-addition of 50 scans.

Prior to catalytic tests, the catalysts were pre-treated from 25 to 500 °C under 5% O_2/He (*ν* = 20 °C/min) to remove most of adsorbed impurities. After cooling down to 30 °C (under He), the standard gas mixture was sent through the catalyst and the temperature was increased from 25 to 500 °C (TPSR experiments, *ν* = 5 °C/min). Then, the temperature was decreased progressively from 500 to 150 °C by dwells of 50 °C to measure the SCR activity of the catalysts under steady-state conditions (in our conditions after 1 h at each temperature).

3. Results and discussion

In the first place, the Ag-based catalysts structural properties will be addressed by application of PXRD, Raman Spectroscopy and TEM. Then, their performance in NO_x SCR with ethanol will be presented. In the light of the results obtained on the catalytic activity, the catalysts relative reducibility and acidity were accessed by H_2-TPR, DRS UV–Vis Spectroscopy, CO adsorption followed by DRIFTS and pyridine adsorption followed by FTIR.

3.1. Ex situ structural characterization techniques

3.1.1. Powder XRD

Application of this technique to the four catalysts provides information on the possible presence of Ag crystalline phases (*e.g.* AgO, Ag_2O, Ag_2SO_4, Ag^0 and, only for Ag/Al_2O_3, silver aluminate [7]).

Fig. 1 shows the PXRD patterns of 2.5Ag/Al_2O_3, 3Ag/CZ and 4Ag/HMFI(25) catalysts and of the respective calcined supports prior to Ag introduction (Al_2O_3, CZ, SCZ and HMFI(25)).

Regarding 2.5Ag/Al_2O_3 catalyst, no diffraction peaks corresponding to an Ag crystalline phase were detected. This observation is in line with the work of Sayah et al. [28], who also did not found any evidence of these species in the PXRD pattern of a calcined 2.5Ag/Al_2O_3 sample prepared under similar conditions. However,

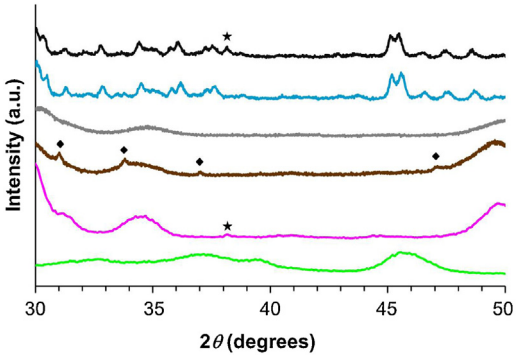

Fig. 1. PXRD patterns of 2.5Ag/Al_2O_3 ( ), CZ ( ), 3Ag/CZ ( ), SCZ ( ), 3Ag/SCZ ( ), 3Ag/SCZ after the catalytic test ( ), HMFI(25) ( ), 4Ag/HMFI(25) ( ) and 4Ag/HMFI(25) after the catalytic test ( ). (For interpretation of the references to color in this figure legend, the reader is referred to the web version of this article.)

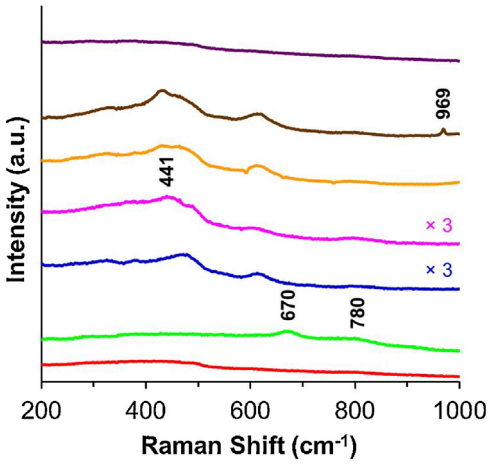

Fig. 2. Raman spectra at RT of Al_2O_3 ( ), 2.5Ag/Al_2O_3 ( ), CZ ( ), 3Ag/CZ ( ), SCZ ( ), 3Ag/SCZ ( ) and HMFI ( ). (For interpretation of the references to color in this figure legend, the reader is referred to the web version of this article.)

it should be noted that some uncertainty remains due to overlapping of the main diffraction peaks of metallic silver with those of the support and the grey color of 2.5Ag/Al_2O_3, which contrasts with the white color of Al_2O_3. Thus, the presence of small Ag_2O and/or Ag^0 crystallites non-detected by PXRD cannot be excluded.

Contrarily to 2.5Ag/Al_2O_3, a small diffraction peak at $2\theta = 38.1^\circ$ was observed in the PXRD pattern of 3Ag/CZ, probably indicating the presence of Ag^0 particles on this catalyst. In fact, Aneggi et al. [29] have performed *in situ* XRD during the calcination of a 5 wt% Ag/CeO_2 sample and observed the formation of Ag^0 particles. Further characterization by TEM has confirmed that these particles were formed by thermal reduction of pseudo-amorphous Ag_2O domains, themselves in direct contact with CeO_2 crystallites.

The PXRD pattern of 3Ag/SCZ was already analysed by Westermann et al. [10]. The major conclusion of this analysis was the detection of a crystalline Ag_2SO_4 phase on 3Ag/SCZ. The formation of Ag_2SO_4 is due to a surface reaction during the impregnation or calcination steps between the ionic sulphate species present on the support under "wet" conditions and the silver salt. After a NO_x SCR test with C_2H_5OH, the presence of Ag_2SO_4 was no longer detected in the PXRD pattern, which proves that this phase is unstable under reaction conditions.

Regarding 4Ag/HMFI, no Ag crystalline phases were detected on the white 4Ag/HMFI(25) catalyst. However, it should be pointed out that weak but discernible diffraction lines that can be assigned to Ag^0 were detected on 4Ag/HMFI after a NO_x SCR test with C_2H_5OH.

So, to summarize PXRD observations on the as-prepared catalysts, only on 3Ag/CZ and on 3Ag/SCZ this technique detected the presence of Ag phases, namely Ag^0 and metastable Ag_2SO_4 particles, respectively.

Finally, it should be noted that, due to the detection limits of PXRD, the non-observation of diffraction peaks of a given Ag species does not exclude its presence. In fact, XRD detection limits depend mostly on the diffraction domain (particle size) as well as on the concentration of a given crystalline phase.

3.1.2. Raman spectroscopy

The structural characterization by PXRD was complemented by Raman spectroscopy. First, it has to be outlined that it was impossible to obtain reliable spectra for 4Ag/HMFI catalyst due to strong fluorescence effects at the laser wavelength used.

Nevertheless, the Raman spectra of the other Ag-based catalysts are compared with those of their corresponding supports on Fig. 2.

The spectrum of 2.5Ag/Al_2O_3 catalyst displays two new bands at 670 and 780 cm^{-1}, not observed for the Al_2O_3 support. In the literature, rather contradictory data exist for the Raman identification of Ag_2O and even AgO oxides due to the photosensitivity of these products (namely the former) to some light wavelengths. According to Waterhouse et al. [30], the main spectral feature of Ag_2O is a weak and broad band whose maximum lays in the 410–530 cm^{-1} range, while AgO displays a rather sharp peak at 430 cm^{-1} accompanied by weaker features at 217, 300, 375, 467 and 488 cm^{-1}. None of these spectral features matches those of 2.5Ag/Al_2O_3. In fact, the bands at 670 and 780 cm^{-1} are more consistent with some vibrations modes of sub-surface and surface oxygen, chemisorbed on a metallic silver phase arising from the thermal decomposition of Ag_2O [31].

The Raman spectra of CZ and SCZ supports exhibit the characteristic spectral features of $Ce_xZr_{1-x}O_2$ solid solutions with tetragonal structures. The sulphation of the support influences the nature of the supported Ag phases, as already deduced from PXRD. 3Ag/SCZ catalyst presents a fine peak at 969 cm^{-1}, which is well characteristic of an Ag_2SO_4 phase [32]. As for 3Ag/CZ, rather broad peaks are also observed around 430–450 cm^{-1} that can be tentatively assigned to AgO or Ag_2O (AgO_x) species.

To sum up, structural characterization of the calcined catalysts by PXRD and Raman spectroscopy seemed to reveal the presence of defective Ag^0 particles surrounded by strongly chemisorbed oxygen atoms for 2.5Ag/Al_2O_3, mixed Ag^0/AgO_x species for 3Ag/CZ and an Ag_2SO_4 phase co-existing with Ag^0/AgO_x entities for 3Ag/SCZ. Exchanged Ag^+ species which are thought to be dominant on 4Ag/HMFI are not detected by these techniques.

3.1.3. TEM

TEM micrographs of the four Ag-based catalysts are reported in Fig. 3.

First, 2.5Ag/Al_2O_3 TEM micrographs do not show any evidence of the presence of Ag particles. This implies that silver is highly dispersed over the Al_2O_3 support, which is in line with the PXRD results and with the observations of Musi [33] on a similar 2.5Ag/Al_2O_3 catalyst.

Concerning 3Ag/CZ, although CZ inter-reticular plane (1 0 1) was identified, the TEM micrograph of this catalyst does not evidence the presence of Ag particles, which were detected on this catalyst by PXRD (*vide supra* Section 3.1.1). However, Hickey et al. [34] also did not observe the presence of Ag particles on a CZ ($Ce_{0.16}Zr_{0.84}O_2$) with 2 wt% Ag. The authors explained this fact with the poor contrast of Ag particles in the CZ support, which can possibly hinder the detection of small Ag^0 and/or Ag_2O particles. On the other hand,

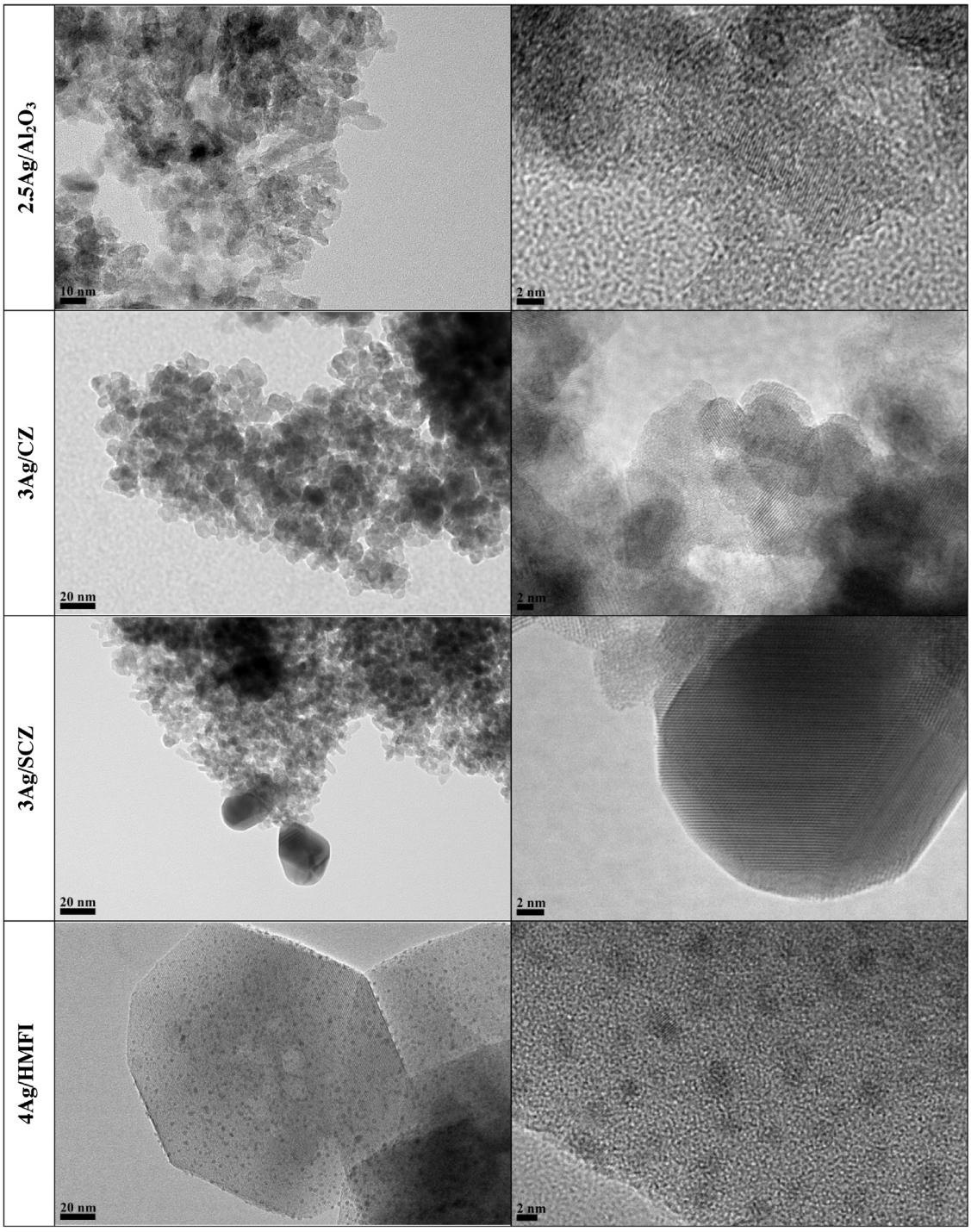

Fig. 3. TEM micrographs of $2.5Ag/Al_2O_3$, 3Ag/CZ, 3Ag/SCZ and 4Ag/HMFI.

according to Aneggi et al. [29], HR-TEM of a 5 wt% Ag/CeO_2 catalyst detected the presence of Ag_2O particles in contact with CeO_2 and Ag^0 particles in contact with Ag_2O particles. These authors explained this finding by the fact that Ag_2O reduction to metallic silver is delayed in the presence of CeO_2. The significantly lower Ag content of 3Ag/CZ in conjugation with the presence of ZrO_2 can explain the differences in the Ag particles observed on 3Ag/CZ when compared to the work of Aneggi et al. [29].

In contrast with the previous two catalysts, TEM analysis detected the presence of Ag particles on 3Ag/SCZ and 4Ag/HMFI. TEM measurements further confirmed that these particles correspond to Ag^0: an inter-reticular plane distance of 3.36 Å, corresponding to place (1 1 1) of face-centred cubic (FCC) metallic silver was found in these particles. However, the morphology of Ag^0 particles is quite different for 3Ag/SCZ and 4Ag/HMFI catalysts. While on 3Ag/SCZ the metallic particles are scarce and have a diameter around 20 nm with a non-spherical shape, on 4Ag/HMFI spherical Ag^0 particles are present in a far greater amount and with a mean diameter of 2 nm (obtained by counting 200 particles diameters).

Regarding 3Ag/SCZ, TEM results, which indicate the presence of Ag^0 particles and the absence of Ag_2SO_4 phase, seem to contradict

the PXRD and Raman results presented in Sections 3.1.1 and 3.1.2, respectively. However, this discrepancy can be simply explained by a reduction under vacuum and/or the electron beam, inside the microscope, of Ag_2SO_4 into Ag^0.

Taking into account that for 4Ag/HMFI, according to PXRD, no loss in crystallinity occurred after Ag introduction on the parent zeolite and since the Ag^0 particles are greater than the zeolite pore diameter (2 *vs.* 0.51 nm), it can be concluded that the majority of these particles is located on the outer surface of the zeolite. Ag^0 particles were also detected in a calcined Ag-exchanged X zeolite with 3 wt% Ag by Sayah et al. [35]. However, in addition to the greater particle size (mean diameter above 20 nm), these authors also noticed the presence of Ag_2O particles.

Thus, to summarize, TEM results must be carefully analysed because there is evidence that, at least with 3Ag/SCZ and 4Ag/HMFI, TEM analysis may change the initial Ag species nature on these catalysts, leading to the formation of Ag^0 particles. Even so, this *in situ* reduction process does not occur similarly on all Ag-based catalysts since no Ag^0 particles of comparable size with those detected on 3Ag/SCZ or 4Ag/HMFI were detected on $2.5Ag/Al_2O_3$ and 3Ag/CZ. This can be possibly related with a different initial state and/or a different metal–support interaction of the Ag species present in the different supports prior to TEM analysis.

3.1.4. Summary of Ag species detected by ex situ structural characterization techniques

Table 2 summarizes the Ag species that were detected by the *ex situ* structural characterization techniques, whose results were presented in the previous sections:

Hence, $2.5Ag/Al_2O_3$ has a combination of Ag_2O and reduced Ag^0 species with adsorbed O atoms. These last species with activated adsorbed O atoms have been widely referred as the possible active species in the case of Ag/Al_2O_3 ethylene epoxidation catalysts [36]. Furthermore, in a recent work by Kim et al. [37], reactive oxygen adsorbed onto the surface of an Ag/Al_2O_3 catalyst was also identified by FTIR spectroscopy. A combination of AgO_x/Ag^0 species has been observed on 3Ag/CZ and 3Ag/SCZ, while Ag_2SO_4 particles are also present in the latter case. In the case of 4Ag/HMFI, only Ag^0 particles were detected by TEM analysis. However, it should be noted that these species can be formed by an *in situ* reduction inside the TEM microscope. In addition, although no other Ag species was observed in 4Ag/HMFI, according to the literature [11,38], the presence of Ag^+ species can be postulated in this catalyst.

Table 2
Summary of Ag species detected on the four Ag-containing catalysts according to *ex situ* structural characterization (PXRD + Raman + TEM).

$2.5Ag/Al_2O_3$	3Ag/CZ	3Ag/SCZ	4Ag/HMFI
Ag_2O Ag^0 with ad-O	AgO_x/Ag^0	Ag_2SO_4 AgO_x/Ag^0	Ag^+? Ag^0?

3.2. NO SCR with ethanol catalytic tests

The activity of Ag-containing catalysts activity for NO SCR with ethanol (C_2H_5OH) reaction was evaluated, in order to attempt to establish a relation between the Ag species identified in each catalyst and their NO SCR activity. It is worth outlining that the pre-treated catalysts were submitted first to TPSR tests and then to steady-state isothermal tests. The use of a temperature ramp is useful in detecting activity changes, which could be for instance induced by silver species, among the different catalysts. Fig. 4 shows the TPSR profiles of the four catalysts.

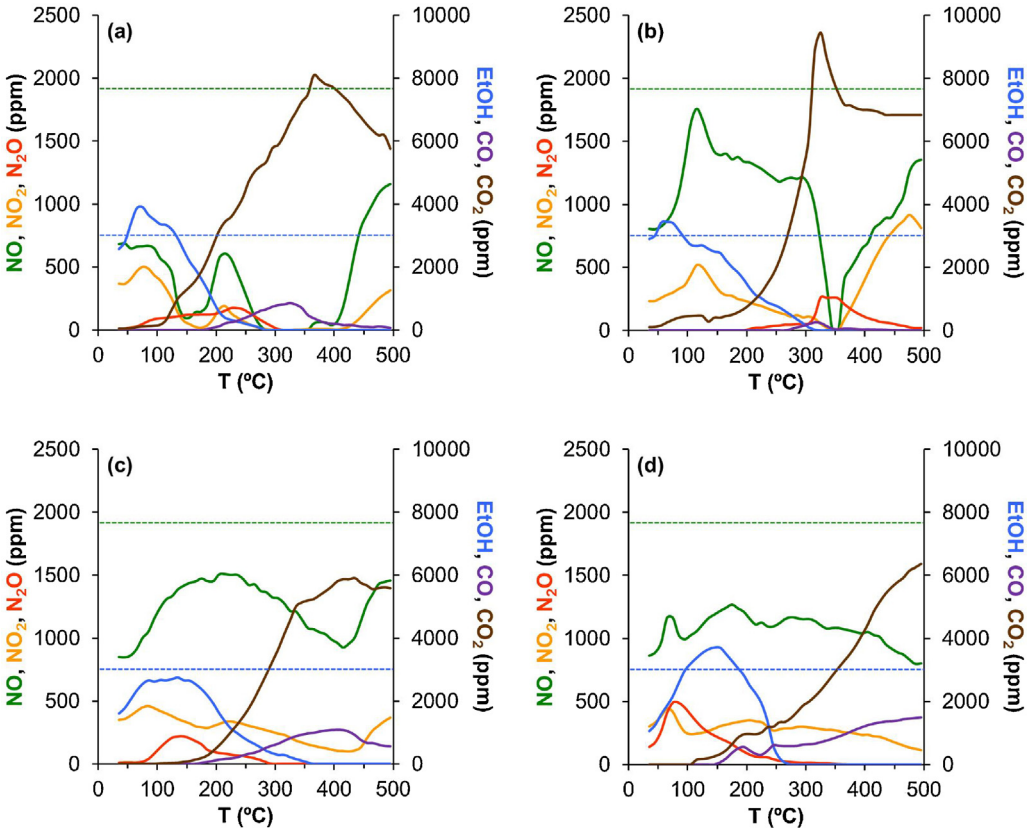

Fig. 4. TPSR profiles of NO (—), NO_2 (—), N_2O (—), C_2H_5OH (—), CO (—) and CO_2 (—) with 1920 ppm NO, 3020 ppm C_2H_5OH and 5% over $2.5Ag/Al_2O_3$ (a), 3Ag/CZ (b), 3Ag/SCZ (c) and 4Ag/HMFI (d). (For interpretation of the references to color in this figure legend, the reader is referred to the web version of this article.)

Clearly, 2.5Ag/Al_2O_3 and 3Ag/CZ are the most efficient catalysts, achieving both 100% NO_x conversion at some temperatures during the TPSR tests. However, while on 2.5Ag/Al_2O_3 the maximum activity window is from 300 to 400 °C, on 3Ag/CZ this window is extremely narrow. On 3Ag/SCZ and on 4Ag/HMFI, maximum NO_x conversion is about 45% at 415 °C and about 50% at 500 °C, respectively. It should be noted that, with the exception of 3Ag/CZ, no N_2O formation is observed above 300 °C. On this catalyst, N_2O formation takes place between 300 and 475 °C, thus coinciding with the maximum NO_x conversion window on 3Ag/CZ. Regarding NO_2 formation, while on 3Ag/SCZ and 4Ag/HMFI it takes place on all the studied temperature range, on 2.5Ag/Al_2O_3 and 3Ag/CZ it occurs mainly below 200 °C and above 400 °C. Moreover, 3Ag/CZ has the highest NO_2 formation among all the four catalysts, with a maximum NO_2 formation of about 915 ppm at 475 °C. It is rather interesting to note that the great NO_2 formation above 400 °C on this catalyst coincides with the decrease in NO_x conversion. Hence, it seems that the loss in NO_x SCR performance of 3Ag/CZ and NO_2 formation are linked. Taking into account the general HC-SCR mechanism proposed by Djéga-Mariadassou [39], two different hypotheses can be advanced to explain this phenomenon. The first one is that the NO_2 formed in the first function stopped reacting in the second function and thus appeared in the TPSR profile of 3Ag/CZ. The second one is that the third function stopped turning and the RNO_x compounds formed in this mechanistic step are instead decomposed into NO_x and CO_x, instead of being converted into N_2.

Concerning ethanol conversion into CO_x, on 2.5Ag/Al_2O_3 and 3Ag/CZ CO formation is low, taking place around 300 °C with a maximum of 850 and 250 ppm, respectively. On the other hand, CO is formed on 3Ag/SCZ and 4Ag/HMFI in a greater amount, above 200 °C (maximum of 1090 and 1500 ppm, respectively). Moreover, CO_2 formation is higher on 2.5Ag/Al_2O_3 and 3Ag/CZ, peaking at the maximum NO_x conversion for all catalysts. However, it should be noted that only on 2.5Ag/Al_2O_3 and 3Ag/CZ catalysts the CO_2 formation exceeds the ethanol concentration fed to the reactor. This evidences a higher formation and adsorption of HC species on the catalysts, possibly enhanced by the Ag species present in these catalysts, which have a high oxidation capacity.

Two additional features of the TPSR tests should be evidenced. The first one regards the low temperature NO_x conversion, around 150 °C, which can be seen on 2.5Ag/Al_2O_3. Given the extremely low temperature range and since the N_2O formed does not correspond to all the consumed NO_x, it can be hypothesized that other NO_x-containing compounds, like RNO_x, are being formed and possibly adsorbed on the catalyst. N_2 formation at quite a low temperature cannot be completely discarded, but should be highly unlikely. Moreover, the formation and adsorption of these compounds on 2.5Ag/Al_2O_3 would explain, at least partially, the high CO_2 formation observed on this catalyst. The second relevant feature is the extremely narrow NO_x conversion window on 3Ag/CZ, around 350 °C. This phenomenon can be explained by a sudden change, at this temperature, in the NO_x SCR reaction mechanism pathway, which can be caused by a modification of the Ag species distribution in this catalyst. In order to better analyse the Ag species stability under NO_x SCR reaction conditions, steady-state isothermal tests were also performed on the four catalysts. These results are depicted in Fig. 5.

While 2.5Ag/Al_2O_3 remains the most active catalyst, with a similar temperature activity window, the high NO_x conversion detected during the TPSR of 3Ag/CZ at 350 °C (Fig. 4b) is lost under steady-state isothermal conditions, with the catalyst activity remaining around 30% on all the studied temperature range. Furthermore, some changes in the maximum NO_x conversion and activity window can be seen for 3Ag/SCZ and 4Ag/HMFI(25). When comparing with TPSR results, in the first case the maximum NO_x conversion decreases to 30% but at a lower temperature, for 4Ag/HMFI(25) maximum NO_x conversion remains unchanged (about 50%), but it is also shifted to a lower temperature (350 °C). Therefore, the most unstable catalyst under reaction conditions, when comparing NO_x conversion into N_2 under TPSR and isothermal steady-state conditions, seems to be 3Ag/CZ, followed by 3Ag/SCZ.

Concerning N_2O, CO and CO_2, their formation during steady-state isothermal conditions follows the same trend observed during TPSR tests. 2.5Ag/Al_2O_3 and 3Ag/CZ have the higher N_2O formation and are more selective towards CO_2, with the lowest light-off temperatures, while 3Ag/SCZ and 4Ag/HMFI are quite selective towards N_2 and have higher CO formation.

Given the fact that a change in the Ag species distribution, which was already hinted by PXRD performed after the NO_x SCR reaction (*vide supra* Section 3.1.1, seems to occur during TPSR experiments, especially on 3Ag/CZ, the Ag species distribution and reducibility on each catalyst will be further analysed in the following sections by other characterization techniques.

3.3. Assessment of Ag species distribution and reducibility by in situ characterization techniques

3.3.1. H_2-TPR

Fig. 6 shows the H_2-TPR profiles of the four Ag-containing catalysts evaluated in this work and of CZ and SCZ supports.

In contrast with CZ and SCZ, Al_2O_3 and HMFI supports do not exhibit any H_2 consumption process. Hence, for brevity's sake, they were not shown.

The H_2-TPR profile of 2.5Ag/Al_2O_3 distinguishes itself from all the other Ag-based catalysts, since it does not show any H_2 consumption process. This is not in line with the results of Musi et al. [2], who observed a reduction process around 300 °C on several Ag/Al_2O_3 catalysts after a pre-treatment with 10% O_2/He at 500 °C. However, it should be emphasized that when the pre-treatment temperature was lowered to 250 °C (instead of 500 °C), an H_2 consumption peak, with maximum at 130 °C, was detected. Thus, the observation of the Ag species present on 2.5Ag/Al_2O_3, by H_2-TPR, is highly dependent on the pre-treatment conditions, namely the temperature. A similar feature was observed by Richter et al. [40] with an Ag_2O/α-Al_2O_3 mechanical mixture. These authors found that, when this sample was pre-treated with air at 500 °C, no H_2 consumption occurs, while after a pre-treatment with an inert gas at 100 °C, a reduction peak appears at 180 °C. This result was explained by the Ag_2O thermal decomposition to Ag^0 (under air flow, bulk Ag_2O decomposes around 350–400 °C [30,41]). Therefore, given the fact that no reduction peak is observed in the H_2-TPR of 2.5Ag/Al_2O_3, the Ag_2O (or other oxide phase) reduction to Ag^0 has probably occurred during the pre-treatment with air at 500 °C.

Regarding the CZ support, this material has two reduction peaks, at around 360 and 555 °C. Adamowska et al. [42] reported a similar H_2-TPR for a CZ with 85% CeO_2 and 15% ZrO_2, which also has two reduction peaks, around 375 and 525 °C. The authors attributed these H_2 consumption processes to a stepwise reduction of surface (the first reduction peak) and then bulk (the second reduction peak) Ce^{4+} to Ce^{3+}. A similar interpretation was proposed previously by Giordano et al. [43] for the presence of two reduction processes on CeO_2.

When Ag is introduced in this support, two low-temperature reduction peaks at 85 and 165 °C appear on the H_2-TPR profile of the resulting 3Ag/CZ catalyst. Aneggi et al. [29] reported a broad reduction peak at about 105 °C on CeO_2 containing 5 wt% Ag, attributed to Ag_2O reduction. Since CZ does not have exchange-sites to stabilize isolated Ag^+ ions in the same manner as zeolites, the two reduction peaks on 3Ag/CZ can tentatively be assigned to AgO (peak at 85 °C) and Ag_2O (peak at 165 °C) reduction. This attribution is further supported by the fact that Ag_2O_3, an Ag oxide which, along

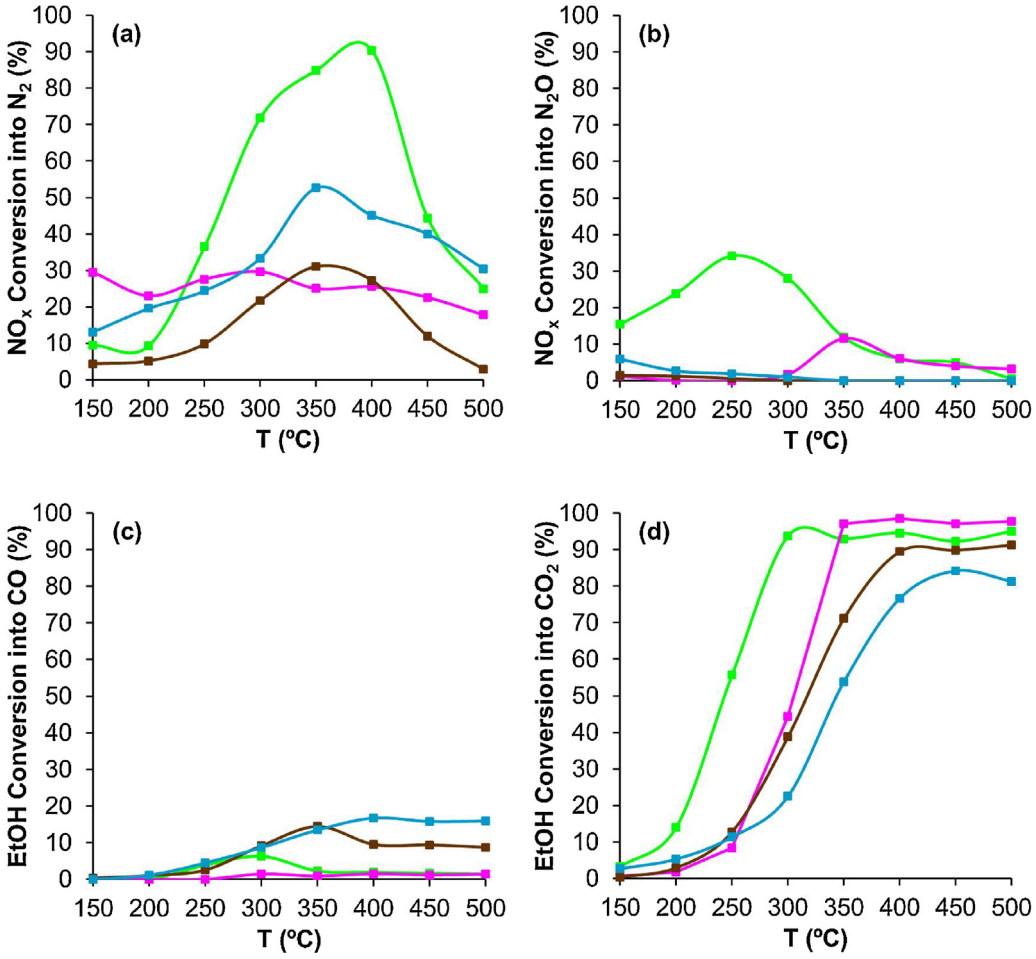

Fig. 5. Isothermal steady-state NO_x conversion into N_2 (a) or N_2O (b) and ethanol conversion into CO (c) and CO_2 (d) with 1920 ppm NO, 3020 ppm ethanol and 5% over 2.5Ag/Al_2O_3 ( ), 3Ag/CZ ( ), 3Ag/SCZ ( ) and 4Ag/HMFI ( ). (For interpretation of the references to color in this figure legend, the reader is referred to the web version of this article.)

with Ag_2O, is present in the composition of the mixed oxide AgO, is reduced at around 90 °C [15]. The high oxygen storage capacity of CZ support would also allow an easy donation of active oxygen atoms towards Ag, hence contributing towards AgO stabilization. Moreover, when comparing CZ and 3Ag/CZ H_2-TPR profiles, it can be seen that the support reduction peaks decrease in the case of 3Ag/CZ, due to Ag presence. This suggests withdrawal of at least a part of the active oxygen from the support, caused by the Ag species present on 3Ag/CZ, which act as an oxygen porthole.

Moving on to SCZ support H_2-TPR profile, a dominant H_2 consumption process with maximum at 615 °C can be seen in Fig. 6, which can be attributed to: (i) surface sulfate reduction, leading to SO_2 and/or H_2S formation [44] and (ii) once the grafted sulfates are eliminated, the reduction of the underlying ceria–zirconia oxide takes place immediately. In other words, SCZ reducibility is smaller than for CZ due to the presence of surface sulphates that hinder the oxygen mobility. When Ag is introduced in this support, this reduction peak is shifted to 500 °C, as it can be seen in the H_2-TPR profile

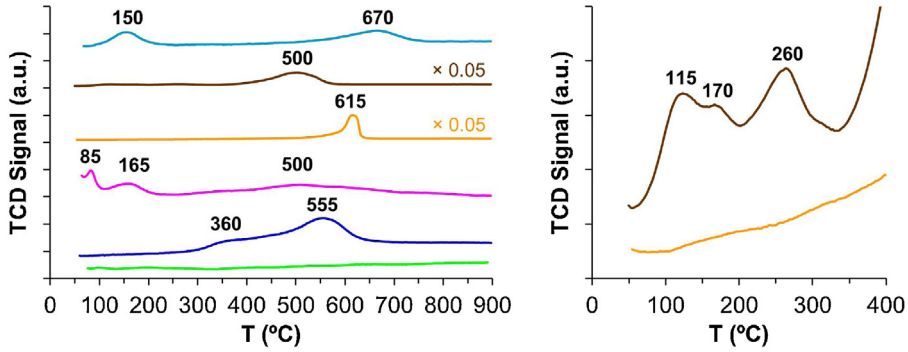

Fig. 6. H_2-TPR profiles of 2.5Ag/Al_2O_3 ( ), CZ ( ), 3Ag/CZ ( ), SCZ ( ), 3Ag/SCZ ( ) and 4Ag/HMFI ( ), and magnification of the low-temperature H_2-TPR profiles of SCZ and 3Ag/SCZ. All samples were pre-treated under air at 500 °C prior to the H_2-TPR runs. (For interpretation of the references to color in this figure legend, the reader is referred to the web version of this article.)

of 3Ag/SCZ. This shift to a lower temperature can be explained by the presence of Ag, onto which H_2 dissociates and then spills-over to the support, facilitating the SO_4^{2-} reduction reaction. Indeed, Schins et al. [45] found evidence of H_2 dissociation over Ag^0, which supports this hypothesis.

In addition to the SO_4^{2-} reduction peak, 3Ag/SCZ has three low-temperature reduction processes at 115, 170 and 260 °C (see magnification of H_2-TPR low temperature region shown in Fig. 6). As can be seen by comparison with SCZ, these H_2 consumption processes are not present on the support and thus can be ascribed to Ag species reduction. Regarding these peaks attributions, a similar reasoning of that used for 3Ag/CZ can be applied to this catalyst. Therefore, the peak at 115 °C would correspond to Ag_2O_3 reduction, indicating the presence of AgO, while the peak at 170 °C can be ascribed to Ag_2O reduction. The third H_2 consumption process, at 260 °C can be ascribed to Ag_2SO_4 reduction, an oxidized Ag species previously identified on this catalyst by PXRD analysis [10]. According to Habashi et al. [46], bulk Ag_2SO_4 starts to reduce around 260 °C, which is in agreement with the temperature of the third reduction peak on 3Ag/SCZ. Moreover, according to these authors, bulk Ag_2SO_4 is stable under air or inert atmosphere up to 800 °C, thus the sample pre-treatment does not have any effect on this species prior to the H_2-TPR experiment.

The H_2-TPR profile of 4Ag/HMFI, exhibits two main H_2 consumption processes with maxima at 150 and 670 °C. This feature is rather common to other Ag/MFI zeolites and has already been reported by several authors [20,47,48]. The first reduction peak corresponds to the reduction of Ag^+ to $Ag_n^{\delta+}$ which are then reduced on the second H_2 consumption process to Ag_m and/or Ag^0 [20].

Lastly, the relative order of H_2 consumption between the four Ag-based catalysts obtained by integration of the H_2 consumption peaks of each catalyst in a.u. is the following: 4Ag/HMFI(25) > 3Ag/SCZ > 3Ag/CZ > 2.5Ag/Al_2O_3 = 0. Therefore, after a pre-treatment at 500 °C under an air flow, the amount of oxidized Ag species on the prepared catalysts follows this order.

3.3.2. DRS UV–Vis spectroscopy

As it was mentioned in our previous study on Ag-exchanged L zeolites [27], UV–Vis band attribution of the different Ag species varies greatly in the literature, namely concerning distinction between $Ag_n^{\delta+}$ and Ag_m species, which have been reported to absorb radiation in the range 240–350 nm. In addition, Ag_2O detection by UV–Vis spectroscopy is not possible [26]. Nonetheless, Ag^+ (208–238 nm) and Ag^0 (above 350 nm) band attribution is relatively consensual and, as such, DRS UV–Vis is widely used for Ag species characterization on Ag-based catalysts.

The DRS UV–Vis spectra of 2.5Ag/Al_2O_3 and 4Ag/HMFI during a pre-treatment with air at 500 °C and subsequent reduction under 5% H_2/He at 500 °C are presented in Fig. 7. It should be noted that this procedure is identical to the one used during H_2-TPR experiments.

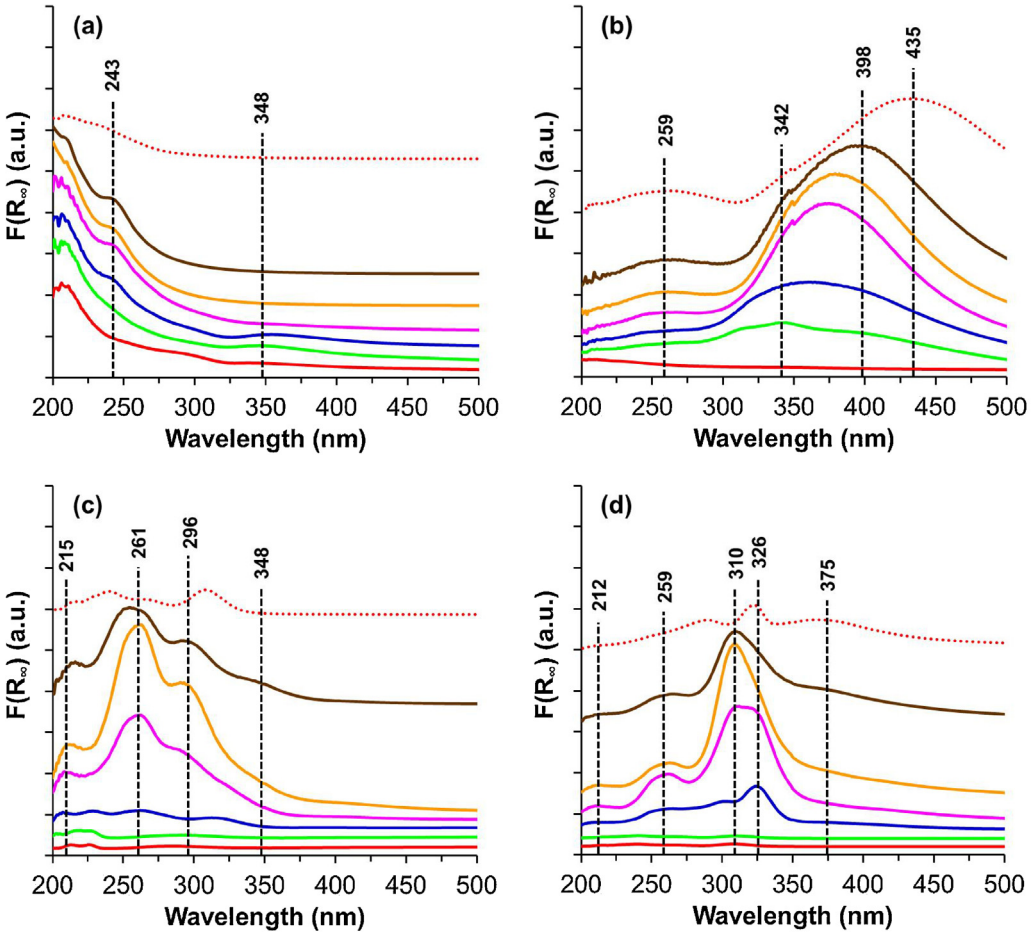

Fig. 7. Diffuse reflectance UV–Vis spectra at RT ( ), 100 °C ( ), 200 °C ( ), 300 °C ( ), 400 °C ( ), 500° ( ) and RT after heating at 500 °C ( ) of 2.5Ag/Al_2O_3 during pre-treatment under air up to 500 °C (a) and subsequent reduction under 5% H_2/He up to 500 °C (b) and of 4Ag/HMFI during pre-treatment under air up to 500 °C (c) and subsequent reduction under 5% H_2/He up to 500 °C (d). (For interpretation of the references to color in this figure legend, the reader is referred to the web version of this article.)

Starting with 2.5Ag/Al_2O_3 (Fig. 7a) this catalyst shows, at RT and prior to any treatment, a broad absorption from 200 to 250 nm, in which Ag^+ have been reported to absorb [2,49]; however the presence of clear absorption bands cannot be observed. When 2.5Ag/Al_2O_3 undergoes the oxidation treatment, at 100 °C, a small band with maximum at 348 nm appears, but then disappears at 300 °C. This band can be ascribed to $Ag_n^{\delta+}$ or Ag_m species [2,7,50]. Furthermore, another small band with maximum at 243 nm, which can be attributed to Ag^+ [3,18], appears at 200 °C, disappearing at RT, after the oxidation treatment. Nonetheless, in spite of these small bands, the spectra of 2.5Ag/Al_2O_3 remain fairly similar throughout the oxidation treatment. However, it should be noted that the catalyst color changed from grey to white, which can be ascribed to the possible Ag_2O decomposition under oxidizing conditions referred previously in Section 3.3.1. After this pre-treatment under air, when 2.5Ag/Al_2O_3 is reduced under 5% H_2/He (in Fig. 7b), a broad absorption with maximum at 398 nm appears at 100 °C and considerably increases, while shifting to 435 nm at RT, after being heated to 500 °C. Since this band can be ascribed to Ag^0 particles [2], the reduction treatment followed by DRS UV–Vis spectroscopy seems to indicate that an Ag species reduction occurs on 2.5Ag/Al_2O_3, although no H_2 consumption was detected by H_2-TPR. Furthermore, since this reduction seems to start below 100 °C, it can be hypothesized that Ag reduction occurs at a rather low temperature, possibly immediately after the 5% H_2/Ar mixture is introduced in the H_2-TPR reactor. In this case, the increase in the Ag^0 absorption band above 100 °C would correspond to the thermal aggregation of Ag^0 particles already formed at RT, proceeding without H_2 consumption and thus being not visible by H_2-TPR. Nonetheless, the hypothesis of Ag_2O decomposition that would occur during the oxidation treatment, advanced in Section 3.3.1, cannot be discarded. Although no significant changes can be detected in the DRS UV–Vis spectra during the oxidation pre-treatment, in Section 3.3.1 it was clearly demonstrated the pre-treatment influence on the reducibility of the Ag species present on 2.5Ag/Al_2O_3.

4Ag/HMFI catalyst, on the other hand, has different spectral features when compared to 2.5Ag/Al_2O_3. It can be seen that, at RT (Fig. 7c), the only Ag species detected on this catalyst is Ag^+ (band at 215 nm) [38]. At 300 °C under air flow, however, two bands at 261 and 296 nm appear, decreasing at 500 °C but still being retained at RT, after the oxidation treatment. According to the literature, these bands can be ascribed to $Ag_n^{\delta+}$ [20] and Ag_m [51], respectively. When 4Ag/HMFI is reduced under 5% H_2/He (Fig. 7b), a band at 326 nm appears at 200 °C, which can be attributed to $Ag_n^{\delta+}$ species [52]. This in line with the first reduction peak of 4Ag/HMFI, with maximum at 150 °C, as reported in Section 3.3.1. This band further increases up to 400 °C, shifting to 310 nm, being retained at RT, after the reduction treatment. Thus, although reduction at 500 °C of 2.5Ag/Al_2O_3 leads to the formation of Ag^0 particles, the same does not hold true to 4Ag/HMFI, whose reduction at 500 °C leads instead to the formation of $Ag_n^{\delta+}$ species. It should be noted that a small band at 375 nm, which can be ascribed to Ag^0 particles [38], also appears at 500 °C on 4Ag/HMFI, being retained at RT, after the reduction treatment.

Spectra of 3Ag/CZ and 3Ag/SCZ were also collected, but, due to the strong absorption of the CZ and SCZ supports between 200 and 400 nm (which coincides with the range in which the different Ag species can be found), Ag species detection by DRS UV–Vis is severely hindered. Due to lack of information that can be obtained on the Ag species present on 3Ag/CZ and 3Ag/SCZ, DRS UV–Vis spectra of these catalysts are not presented. The strong absorption mentioned above was also found by other authors [53–55] on ceria–zirconia-based catalysts and it can be attributed mainly to $Ce^{3+} \leftarrow O^{2-}$, $Ce^{4+} \leftarrow O^{2-}$ and $Zr^{2+} \leftarrow O^{2-}$ charge transfer transitions. Nonetheless, absorptions on the range 400–450 nm, which can be ascribed to Ag^0, can be observed during the oxidation and the reduction treatments of 3Ag/CZ, signalling the high reducibility of the oxidized Ag species present on this catalyst.

3.3.3. *In situ DRIFTS of adsorbed CO*

The primary aim is to probe with FTIR of adsorbed CO the electronic state of supported silver species, with the basic idea that: the more electron-deficient is the Ag species, the highest will be the frequency of adsorbed CO. According to Hadjiivanov and Vayssilov [56], at room temperature, CO can only be adsorbed on Ag^+ species and this adsorption takes place between 2200 and 2151 cm^{-1}; Ag^0 can also adsorb CO, but only at low temperature and outside of the aforementioned spectral range, at 2060 cm^{-1}. However, it should also be taken into consideration that, according to some authors [57], CO adsorption on Ag_2O, which contains unsaturated Ag^+ sites, is also possible. Furthermore, assuming that CO can adsorb in Ag_2O, then it can also be assumed that CO adsorption in Ag_2SO_4 is also possible. The reasoning supporting this statement is that, due to the higher electronegativity of SO_4^{2-} when compared to O^{2-}, Ag^+ sites on Ag_2SO_4 are more electro-deficient than those on Ag_2O, thus CO adsorption will be easier.

To summarize, it can be stated that, when performed at room temperature, CO adsorption on Ag-containing catalysts can be used to probe oxidized Ag species, namely Ag^+ and possibly also Ag_2O and Ag_2SO_4.

Thus, CO adsorption was performed on the four Ag-containing catalysts prepared in this work and followed by DRIFTS. The results obtained can be seen in Fig. 8.

From their overall spectral features, the previous spectra can be grouped in two sets: 2.5Ag/Al_2O_3 and 3Ag/CZ *vs.* 3Ag/SCZ and 4Ag/HMFI. CO adsorption on the first catalysts set produces a weak band at 2164 cm^{-1} on 2.5Ag/Al_2O_3, which is in agreement with the work of Richter et al. [40], and at 2161 cm^{-1} on 3Ag/CZ. On the other hand, on the second set, CO adsorption results in fairly strong bands at higher wavenumbers: 3Ag/SCZ has a band at 2179 cm^{-1} while 4Ag/HMFI(25) has two bands at 2182 and 2191 cm^{-1}. At low CO coverage (t = 3, 10 min on Fig. 8d), this last band is predominant, whereas with increasing CO coverage the band at 2182 cm^{-1} becomes stronger than that at 2191 cm^{-1}. It should be noted that the significantly greater adsorbed CO band intensity on 3Ag/SCZ and 4Ag/HMFI when compared with 2.5Ag/Al_2O_3 and 3Ag/CZ may hint to a higher dispersion and/or amount of oxidized Ag species in the two former catalysts.

Furthermore, the band position of the absorbed CO on the four Ag-based catalysts allows to conclude that the Ag species onto which CO is adsorbed have the following electron-deficiency order: 3Ag/CZ ~ 2.5Ag/Al_2O_3 < 3Ag/SCZ < 4Ag/HMFI. It should be noted that this order follows the relative H_2 consumption order found by H_2-TPR (*vide supra* Section 3.3.1). The proximity of the two wavenumbers of adsorbed CO on 3Ag/CZ and 2.5Ag/Al_2O_3 seems to indicate a similar electro-deficiency and thus a rather similar type of Ag species. Since the presence of reducible oxidized species was assessed from H_2-TPR measurements (*vide supra* Section 3.3.1) on both catalysts, these oxidized Ag species may be assumed to arise from a kind of supported Ag_2O or Ag^0/AgO_x species. In the case of 3Ag/SCZ, with a higher adsorbed CO frequency, it can be hypothesized that CO on this catalyst is adsorbed on Ag_2SO_4, which was detected by PXRD [10]. On 4Ag/HMFI, with the highest adsorbed CO wavenumber, CO should be adsorbed on Ag^+ located on the zeolite exchange-sites, which were also detected by H_2-TPR (*vide supra* Section 3.3.1).

It should be stressed out that the electro-deficiency of these oxidized Ag species supports the order $Ag_2O < Ag_2SO_4 < Ag^+$, which agrees with the adsorbed CO wavenumber on the four Ag-based

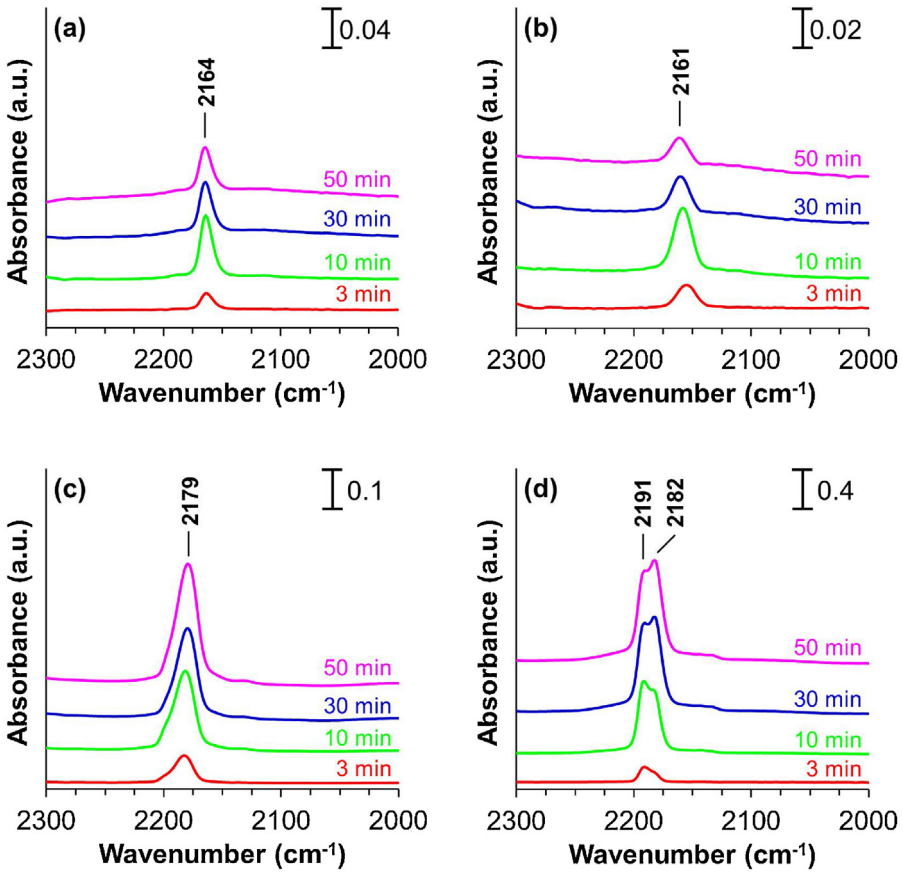

Fig. 8. DRIFTS spectra of adsorbed CO (flow of 1000 ppm/He) on 2.5Ag/Al_2O_3 (a), 3Ag/CZ (b), 3Ag/SCZ (c) and 4Ag/HMFI (d) at different adsorption times.

catalysts. In addition, according to theoretical calculations performed by Casarin et al. [57], CO adsorbed on Ag_2O would have a band at 2158 cm^{-1}, which is in good agreement with the bands at 2164 and 2161 cm^{-1}, observed on 2.5Ag/Al_2O_3 and on 3Ag/CZ, respectively. Moreover, Hadjiivanov and Vayssilov [56] reported that a band at 2170 cm^{-1} appears on Ag_2O/Al_2O_3 after CO adsorption, which also supports the previous band attribution on 2.5Ag/Al_2O_3.

In order to perform a semi-quantitative comparison of the adsorbed CO amount on the different catalysts, the adsorbed CO bands represented in Fig. 8 can be integrated and represented as a function of the adsorption time, as depicted in Fig. 9.

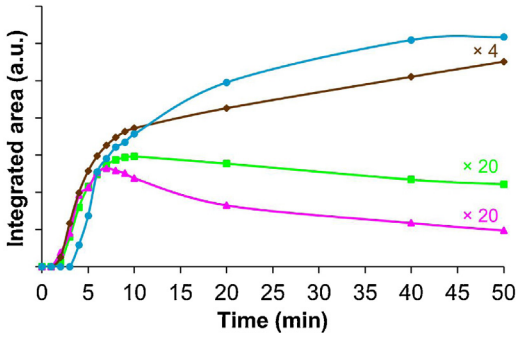

Fig. 9. Evolution of the integrated CO bands *vs.* time for 2.5Ag/Al_2O_3 (▬), 3Ag/CZ (▬), 3Ag/SCZ (▬) and 4Ag/HMFI (▬). For clarity sake, the 2.5Ag/Al_2O_3 and 3Ag/CZ integrated areas were multiplied by 20, while the 3Ag/SCZ integrated areas were multiplied by 4. (For interpretation of the references to color in this figure legend, the reader is referred to the web version of this article.)

Analysing the evolution of the integrated CO bands *vs.* time, (Fig. 9), in a similar manner to what was done for the DRIFTS spectra of adsorbed CO (Fig. 8), two catalysts sets can be identified: 2.5Ag/Al_2O_3 and 3Ag/CZ *vs.* 3Ag/SCZ and 4Ag/HMFI.

The first catalyst group is characterized by lesser apparent amounts of CO adsorbed and by a decrease of the adsorbed CO amount that starts around 10 min. This can be explained by a possible reduction of Ag^0/AgO_x species, on which the CO molecules are adsorbed, to Ag^0, on which CO does not adsorb at RT, according to the following reaction:

$$Ag_2O + CO \rightarrow Ag^0 + CO_2 \quad (1)$$

Moreover, this reaction has already been observed by Lim et al. [58] for CO adsorption on Ag_2O nanoparticles supported on Highly Ordered Pyrolytic Graphite (HOPG). Nevertheless, clearly the oxidized Ag species present on 2.5Ag/Al_2O_3 and 3Ag/CZ are more easily reduced than those present on 3Ag/SCZ and 4Ag/HMFI. In contrast with the results presented in this work regarding CO adsorption on 2.5Ag/Al_2O_3, Bechoux et al. [59] did not observe a decrease in the CO adsorbed on an Ag/Al_2O_3 catalyst. However, it should be noted that these authors did not perform the CO adsorption under flowing CO, but rather by introduction of calibrated aliquots, which, in addition, led to a smaller total CO amount contacted with their catalyst.

On the other hand, 3Ag/SCZ and 4Ag/HMFI are characterized by an increasing CO adsorption on the experiment time span. This seems to signal that, in opposition to the first catalysts set, Ag species reduction caused by the CO probe molecule does not occur. Thus, oxidized Ag species present on 3Ag/SCZ and 4Ag/HMFI have a higher stability than those present on 2.5Ag/Al_2O_3 and 3Ag/CZ.

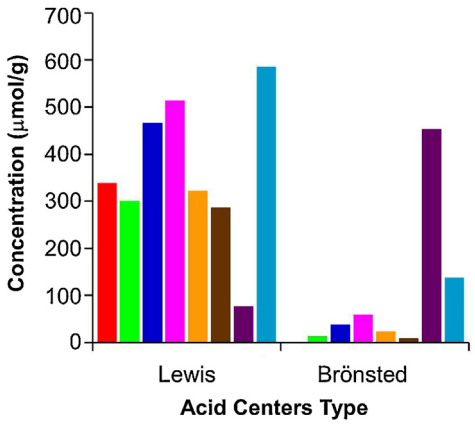

Fig. 10. Concentration of Lewis and Brönsted acid sites on Al_2O_3 ( ), 2.5Ag/Al_2O_3 ( ), CZ ( ), 3Ag/CZ ( ), SCZ ( ), 3Ag/SCZ ( ), HMFI ( ) and 4Ag/HMFI ( ) obtained from pyridine adsorption at 150 °C. (For interpretation of the references to color in this figure legend, the reader is referred to the web version of this article.)

3.3.4. Acidity characterization by pyridine adsorption followed by FTIR

Pyridine adsorption followed by FTIR was used to quantify the different types of acid sites (Lewis or Brönsted), present on the four Ag-based catalysts. Moreover, the effect of Ag introduction on the parent supports acidity was also evaluated by pyridine adsorption on each catalyst calcined parent support, without Ag. This was achieved by integration of the bands around 1450 (Lewis acid sites) and 1540 cm^{-1} (Brönsted acid sites) after pyridine adsorption at 150 °C and by application of the extinction coefficients reported in [60] to the integrated areas. It should be noted that it was assumed that these coefficients do not depend on the solid structure neither on the acid site strength, in line with the observations of Emeis [61]. The concentration of Lewis and Brönsted acid sites for the supports and the Ag-containing catalysts is represented in Fig. 10.

Concerning the four supports analysed, it can be concluded that Lewis acid sites concentration follows the trend: HMFI < SCZ < Al_2O_3 < CZ. On the other hand, the Ag-containing catalysts have the following trend on Lewis acid sites concentration: 3Ag/SCZ < 2.5Ag/Al_2O_3 < 3Ag/CZ < 4Ag/HMFI. It should be stressed out, as it was already discussed above in this section, the great increase in Lewis acid sites concentration of 4Ag/HMFI comparatively to HMFI, while no difference occurs after Ag introduction on the other three supports.

Regarding the Brönsted acid sites concentrations, the only samples having a relevant number of these acid sites are HMFI and 4Ag/HMFI. However, according to the literature [62], SCZ should also have Brönsted acid sites, which were not detected. However, it should be noted that this Brönsted acidity comes from the presence of adsorbed H_2O on the SCZ surface, rendered acidic by the sulphate groups grafted on SCZ, which have an electron-withdrawing effect. Thus, since all samples were pre-treated at 450 °C prior to pyridine adsorption (as described in Section 2.2), this activation procedure removes all the H_2O present on the catalysts and, therefore, also removes the Brönsted acid sites formed on SCZ due to sulphation. This is in line with the work of Davis et al. [63], who observed a decrease in the number of Brönsted acid sites on a sulphated ZrO_2 with the pre-treatment temperature prior to pyridine adsorption.

In a final note, it should be underlined the potentialities of pyridine adsorption on Ag-based catalysts, which, as evidenced in this section for 4Ag/HMFI, is sensible to the type of oxidized Ag species present on Ag-based catalysts. Therefore, based on the increase in Lewis acid sites concentration and the simultaneous decrease in Brönsted acid sites concentration, identification and possibly quantification of certain oxidized Ag species can be done. This technique can be especially useful when trying to ascertain the presence of Ag^+ species, namely for zeolite-based catalysts. In this regard, according to the difference in the Brönsted acid sites concentration between 4Ag/HMFI and HMFI, it can be stated that Ag^+ species account for about 80% of the total Ag present in 4Ag/HMFI.

Table 3
Summary of Ag species detected on the four Ag-containing catalysts according to *in situ* characterization techniques under oxidizing and reducing conditions.

Conditions	2.5Ag/Al_2O_3	3Ag/CZ	3Ag/SCZ	4Ag/HMFI
Oxidizing	Ag_2O? $Ag_n^{\delta+}/Ag_m$	AgO Ag_2O	Ag_2SO_4 AgO? Ag_2O	Ag^+ $Ag_n^{\delta+}$
Reducing	Ag^0	n.d.	n.d.	$Ag_n^{\delta+}$ Ag^0

3.3.5. Ag species detected by in situ characterization techniques: Correlation with NO SCR activity

Table 3 summarizes the Ag species that were detected by the *in situ* characterization techniques, whose results were presented in the previous sections.

Under oxidizing conditions, there are some Ag species whose presence is exclusive of a given catalyst. In this regard, Ag_2SO_4 is only present on 3Ag/SCZ, while only 4Ag/HMFI has Ag^+ species. In an opposite way, Ag_2O is a common species to 2.5Ag/Al_2O_3, 3Ag/CZ and 3Ag/SCZ, while AgO is only present on 3Ag/CZ and 3Ag/SCZ.

On the other hand, under reducing conditions, Ag^0 particles were detected on 2.5Ag/Al_2O_3 and on 4Ag/HMFI, while $Ag_n^{\delta+}$ species, which seem to be majority, were also detected in 4Ag/HMFI.

Although the NO_x SCR with C_2H_5OH reaction is performed in the presence of 7% O_2, thus under oxidizing conditions, the reducing effect of C_2H_5OH on the Ag species, which is presents in a much smaller amount (3020 ppm), cannot be disregarded. According to Sayah et al. [28,64], 3000 ppm C_2H_5OH in gas phase, at temperatures as low as 78 °C, can lead to a reduction of the Ag species on an Ag/Al_2O_3 catalyst, leading to the formation of Ag^0 particles. In this regard, the NO_x SCR reaction mixture can have may have an oxidizing or reducing nature, possibly depending of the reaction temperature.

In addition, it should be also noted that the NO_x SCR reaction is quite complex and comprises several elemental steps, which can be catalysed by different Ag species and even by the support itself.

Taking these considerations into account, analysis of Table 3 allows to conclude that under oxidizing conditions Ag_2O and $Ag_n^{\delta+}/Ag_m$ species were detected on 2.5Ag/Al_2O_3, the most active catalyst for NO_x SCR with ethanol (Figs. 4 and 5). In the literature, oxidized Ag species, like Ag_2O or $Ag_n^{\delta+}$ are typically pointed out as the active species for NO_x SCR. However, the amount of $Ag_n^{\delta+}$ species detected on this catalyst was quite low (*vide supra* Section 3.3.2). In addition, it seems that the Ag_2O species present in 2.5Ag/Al_2O_3 is easily reducible into Ag^0 particles (*vide supra* Section 3.3.1). Hence, a hypothetical Ag_2O/Ag^0 or $Ag_n^{\delta+}/Ag^0$ redox cycle [18] can be hypothesized to occur in this catalyst, under NO_x SCR reaction conditions. Furthermore, the Al_2O_3 support may also play an important role on the formation and/or stocking of intermediate species produced on Ag_2O, as stated by other authors [5,6].

In the case of 3Ag/CZ, containing AgO and Ag_2O under oxidizing conditions, a similar redox cycle can also be postulated. However, in the case of 3Ag/CZ, it seems that the oxidized Ag species can be irreversibly converted into Ag^0 particles, halting the abovementioned redox cycle. This is consistent with the great loss in NO_x conversion and the simultaneous increase in CO_2 formation observed in the TPSR test of this catalyst.

As for 3Ag/SCZ, it seems that the Ag_2SO_4 phase detected under oxidizing conditions is also not stable under NO_x SCR reaction conditions, as confirmed by PXRD (*vide supra* Section 3.1.1). The low activity of this catalyst can then be explained by the fact that a part of its Ag species will be under the form of Ag_2SO_4, which easily decomposes and hence is not able to participate in any redox cycle.

It is also interesting to note that 4Ag/HMFI, which under oxidizing conditions does not have Ag_2O but instead Ag^+ and $Ag_n^{\delta+}$, is the second most active catalyst under steady-state conditions. This evidences that Ag^+ and/or $Ag_n^{\delta+}$ can also catalyze the NO_x SCR reaction, for example by undergoing a redox cycle [11]. Overall, this redox cycle, different from that postulated for $2.5Ag/Al_2O_3$, seems to be less efficient, allowing to attain lower NO_x conversions.

Lastly, it should be mentioned that, in light of the previous discussion on the redox cycles and the changes in the Ag species during the NO_x SCR reaction, it would be relevant to study them under *operando* conditions. Nonetheless, the techniques used in this work were still able to somewhat efficiently probe the Ag species distribution and to give important information about them.

4. Conclusions

NO_x SCR activity with C_2H_5OH of the four Ag-containing catalysts was evaluated under TPSR and steady-state isothermal conditions. Overall, $2.5Ag/Al_2O_3$ is the most efficient catalyst for NO_x conversion into N_2. Another relevant information that was obtained from the catalytic tests was the fact that 3Ag/CZ was also quite active under TPSR conditions, but in a narrow activity window. In addition, this catalyst activity was significantly lower under steady-state conditions. This suggests a possible change in the Ag species distribution, with loss of an active Ag species under reaction conditions.

Application of different characterization techniques performed under *ex situ* and *in situ* conditions allowed identification of the Ag species present on $2.5Ag/Al_2O_3$, 3Ag/CZ, 3Ag/SCZ and 4Ag/HMFI catalysts. This methodology had to be applied since, due to each technique specific limitations, not all Ag species are detected by each technique.

Ex situ structural characterizations revealed the presence of Ag_2O and Ag^0 with ads-O in $2.5Ag/Al_2O_3$, an AgO_x/Ag^0 combination on 3Ag/CZ and 3Ag/SCZ, with also Ag_2SO_4 in this last case. With the exception of Ag^0, detected by TEM but which could come from a partial Ag reduction in the microscope, no Ag species were detected on 4Ag/HMFI by application of *ex situ* structural characterization techniques. This implies that Ag is, at least partially, under the form of Ag^+ in this catalyst.

Further *in situ* characterization techniques were applied to the Ag-based catalysts in order to clarify the possible decomposition phenomenon observed on 3Ag/CZ and to try to establish structure-activity relations between the Ag species and the catalysts activity in NO_x SCR with C_2H_5OH. The possibility of different redox cycles occurring during the NO_x SCR reaction between the silver species present in each catalyst was discussed.

Acknowledgements

The authors wish to thank to Fundação para a Ciência e Tecnologia (FCT) for financial support (grant number SFRH/BD/44108/2008 and project number PTDC/EQU-ERQ/102771/2008).

References

[1] N. Aoyama, K. Yoshida, A. Abe, T. Miyadera, Catalysis Letters 43 (1997) 249.
[2] A. Musi, P. Massiani, D. Brouri, J.-M. Trichard, P. Da Costa, Catalysis Letters 128 (2009) 25.
[3] K. Arve, L. Capek, F. Klingstedt, K. Eranen, L.E. Lindfors, D.Y. Murzin, J. Dedecek, Z. Sobalik, B. Wichterlova, Topics in Catalysis 30 (1) (2004) 91.
[4] F. Thibault-Starzyk, E. Seguin, S. Thomas, M. Daturi, H. Arnolds, D.A. King, Science 324 (2009) 1048.
[5] N. Bion, J. Saussey, C. Hedouin, T. Seguelong, M. Daturi, Physical Chemistry Chemical Physics 3 (2001) 4811.
[6] Y. Yan, Y. Yu, H. He, J. Zhao, Journal of Catalysis 293 (2012) 13.
[7] N. Bogdanchikova, F.C. Meunier, M. Avalos-Borja, J.P. Breen, A. Pestryakov, Applied Catalysis B: Environmental 36 (2002) 287.
[8] K.-i. Shimizu, J. Shibata, H. Yoshida, A. Satsuma, T. Hattori, Applied Catalysis B: Environmental 30 (2001) 151.
[9] A. Westermann, B. Azambre, Catalysis Today 176 (2011) 441.
[10] A. Westermann, B. Azambre, A. Koch, Catalysis Today 191 (2012) 65.
[11] J. Shibata, Y. Takada, A. Shichi, S. Satokawa, A. Satsuma, T. Hattori, Journal of Catalysis 222 (2004) 368.
[12] R. Bartolomeu, C. Henriques, P. da Costa, F. Ribeiro, Catalysis Today 176 (2011) 81.
[13] J. Shibata, Y. Takada, A. Shichi, S. Satokawa, A. Satsuma, T. Hattori, Applied Catalysis B: Environmental 54 (2004) 137.
[14] A. Iglesias-Juez, M. Fernandez-Garcia, A. Martinez-Arias, Z. Schay, Z. Koppany, A.B. Hungria, A. Fuerte, J.A. Anderson, J.C. Conesa, J. Soria, Topics in Catalysis 30 (1) (2004) 65.
[15] T. Furusawa, K. Seshan, J.A. Lercher, L. Lefferts, K.-i. Aika, Applied Catalysis B: Environmental 37 (2002) 205.
[16] K.A. Bethke, H.H. Kung, Journal of Catalysis 172 (1997) 93.
[17] S.G. Aspromonte, R.M. Serra, E.E. Miró, A.V. Boix, Applied Catalysis A: General 407 (2011) 134.
[18] P. Sazama, L. Capek, H. Drobná, Z. Sobalík, J. Dedecek, K. Arve, B. Wichterlová, Journal of Catalysis 232 (2005) 302.
[19] K.-i. Shimizu, K. Sugino, K. Kato, S. Yokota, K. Okumura, A. Satsuma, The Journal of Physical Chemistry C 111 (2007) 6481.
[20] J. Shibata, K.-i. Shimizu, Y. Takada, A. Shichi, H. Yoshida, S. Satokawa, A. Satsuma, T. Hattori, Journal of Catalysis 227 (2004) 367.
[21] V.S. Gurin, N.E. Bogdanchikova, V.P. Petranovskii, Materials Science and Engineering C 18 (2001) 37.
[22] F.C. Meunier, J.P. Breen, V. Zuzaniuk, M. Olsson, J.R.H. Ross, Journal of Catalysis 187 (1999) 493.
[23] S.T. Korhonen, A.M. Beale, M.A. Newton, B.M. Weckhuysen, The Journal of Physical Chemistry C 115 (2011) 885.
[24] W.L. Johnson II, G.B. Fisher, T.J. Toops, Catalysis Today 184 (2012) 166.
[25] J.A. Martens, A. Cauvel, A. Francis, C. Hermans, F. Jayat, M. Remy, M. Keung, J. Lievens, P.A. Jacobs, Angewandte Chemie International Edition 37 (1998) 1901.
[26] M. Richter, A. Abramova, U. Bentrup, R. Fricke, Journal of Applied Spectroscopy 71 (2004) 400.
[27] R. Bartolomeu, R. Bértolo, S. Casale, A. Fernandes, C. Henriques, P. da Costa, F. Ribeiro, Microporous and Mesoporous Materials 169 (2013) 137.
[28] E. Sayah, D. Brouri, Y. Wu, A. Musi, P. Da Costa, P. Massiani, Applied Catalysis A: General 406 (2011) 94.
[29] E. Aneggi, J. Llorca, C. de Leitenburg, G. Dolcetti, A. Trovarelli, Applied Catalysis B: Environmental 91 (2009) 489.
[30] G.I.N. Waterhouse, G.A. Bowmaker, J.B. Metson, Physical Chemistry Chemical Physics 3 (2001) 3838.
[31] B. Pettinger, X. Bao, I. Wilcock, M. Muhler, R. Schloegl, G. Ertl, ChemInform 25 (1994) 85.
[32] I. Martina, R. Wiesinger, D. Jembrih-Simbürger, M. Schreiner, e-Preservation Science 9 (2012) 1.
[33] A. Musi, Réduction des oxydes d'azote en mélange pauvre en utilisant des alcools comme agents réducteurs, in: PhD Thesis, Université Pierre et Marie Curie, Paris, 2008.
[34] N. Hickey, I. Boscarato, J. Kašpar, L. Bertinetti, M. Botavina, G. Martra, Applied Catalysis B: Environmental 100 (2010) 102.
[35] E. Sayah, D. Brouri, A. Davidson, P. Massiani, Studies in Surface Science and Catalysis, 175, Elsevier, Amsterdam, 2010, pp. 711.
[36] M.O. Özbek, R.A. Santen, Catalysis Letters 143 (2013) 131.
[37] P.S. Kim, M.K. Kim, B.K. Cho, I.-S. Nam, S.H. Oh, Journal of Catalysis 301 (2013) 65.
[38] C. Shi, M. Cheng, Z. Qu, X. Bao, Journal of Molecular Catalysis A: Chemical 235 (2005) 35.
[39] G. Djéga-Mariadassou, Catalysis Today 90 (2004) 27.
[40] M. Richter, U. Bentrup, R. Eckelt, M. Schneider, M.M. Pohl, R. Fricke, Applied Catalysis B: Environmental 51 (2004) 261.
[41] S.-W. Baek, J.-R. Kim, S.-K. Ihm, Catalysis Today 93–95 (2004) 575.
[42] M. Adamowska, S. Muller, P. Da Costa, A. Krzton, P. Burg, Applied Catalysis B: Environmental 74 (2007) 278.
[43] F. Giordano, A. Trovarelli, C. de Leitenburg, M. Giona, Journal of Catalysis 193 (2000) 273.
[44] B. de Rivas, C. Sampedro, M. García-Real, R. López-Fonseca, J.I. Gutiérrez-Ortiz, Applied Catalysis B: Environmental 129 (2013) 225.
[45] J.M. Schins, R.B. Vrijen, W.J. van der Zande, J. Los, Surface Science 280 (1993) 145.
[46] F. Habashi, S.A. Mikhail, K.V. Van, Canadian Journal of Chemistry 54 (1976) 3646.
[47] A. Ausavasukhi, S. Suwannaran, J. Limtrakul, T. Sooknoi, Applied Catalysis A: General 345 (2008) 89.

[48] T. Nanba, S. Masukawa, J. Uchisawa, A. Obuchi, Journal of Catalysis 259 (2008) 250.
[49] M. Shimokawabe, A. Kuwana, S. Oku, K. Yoshida, M. Arai, Catalysis Today 164 (2011) 480.
[50] A.N. Pestryakov, A.A. Davydov, Journal of Electron Spectroscopy and Related Phenomena 74 (1995) 195.
[51] Y. Kuroda, T. Mori, H. Sugiyama, Y. Uozumi, K. Ikeda, A. Itadani, M. Nagao, Journal of Colloid and Interface Science 333 (2009) 294.
[52] P. Sazama, H. Jirglová, J. Dedecek, Materials Letters 62 (2008) 4239.
[53] Q. Yu, X. Wu, X. Yao, B. Liu, F. Gao, J. Wang, L. Dong, Catalysis Communications 12 (2011) 1311.
[54] L. Kundakovic, M. Flytzani-Stephanopoulos, Applied Catalysis A: General 183 (1999) 35.
[55] S. Damyanova, B. Pawelec, K. Arishtirova, M.V.M. Huerta, J.L.G. Fierro, Applied Catalysis A: General 337 (2008) 86.
[56] K.I. Hadjiivanov, G.N. Vayssilov, Advances in Catalysis, 47, Academic Press, New York, NY, 2002, pp. 307.
[57] M. Casarin, C. Maccato, A. Vittadini, Chemical Physics Letters 280 (1997) 53.
[58] D.C. Lim, I. Lopez-Salido, Y.D. Kim, Surface Science 598 (2005) 96.
[59] K. Bechoux, O. Marie, M. Daturi, G. Delahay, C. Petitto, S. Rousseau, G. Blanchard, Catalysis Today 197 (2012) 155.
[60] M. Guisnet, P. Ayrault, J. Datka, Polish Journal of Chemistry 71 (1997) 1455.
[61] C.A. Emeis, Journal of Catalysis 141 (1993) 347.
[62] B. Azambre, L. Zenboury, J.V. Weber, P. Burg, Applied Surface Science 256 (2010) 4570.
[63] B.H. Davis, R.A. Keogh, S. Alerasool, D.J. Zalewski, D.E. Day, P.K. Doolin, Journal of Catalysis 183 (1999) 45.
[64] E. Sayah, C. La Fontaine, V. Briois, D. Brouri, P. Massiani, Catalysis Today 189 (2012) 55.